

# Preparation and low temperature stability of PbTe nanocrystals embedded in ZnTe matrix by hot-wall deposition

Seishi Abe<sup>1</sup>

Received: 13 January 2016 / Accepted: 16 April 2016 / Published online: 28 April 2016  
© The Author(s) 2016. This article is published with open access at Springerlink.com

**Abstract** Preparation of PbTe–ZnTe nanocomposite thin film is investigated by one-step synthesis using hot-wall deposition with multiple solid-state resources of PbTe and ZnTe. X-ray diffraction and Raman spectrum indicate that composite thin films contain PbTe with NaCl structure, and ZnTe with zinc-blende structure. High-resolution transmission electron microscopy and fast Fourier transform analysis indicate that isolated PbTe nanocrystalline facets are dispersed in ZnTe matrix. The two compounds phase-separate at hetero-interface without forming a ternary solid solution  $Zn_{1-x}Pb_xTe$ . Therefore, simultaneous evaporation of the multiple resources provides a phase-separating nanocomposite with faceted PbTe nanocrystals embedded in ZnTe matrix. The PbTe crystallizes even at a relatively low substrate temperature of 274 K.

**Keywords** One-step physical synthesis · Nanocomposite thin film · Physical vapor deposition · Simultaneous evaporation · Insoluble material system · High-resolution transmission electron microscopy

## Introduction

Nanoscale semiconductor embedded in a wide-gap material has potential application for quantum dot solar cells due to tunableness for absorbing effective energy region in solar radiation spectrum and impact ionization for producing multiple electron–hole pairs per photon [1].

Nanocomposites with different combinations in nanocrystal and matrix were proposed using chemical or physical preparation techniques [2–9].

A combination of lead and zinc chalcogenide system is valuable for preparing a nanocomposite thin film due to the reasons as follows: (1) this system phase-separates in thermal equilibrium without forming a solid solution, (2) band-gap difference between lead and zinc chalcogenide is relatively large, capable of exhibiting quantum confinement effects, and (3) vapor pressures of lead and zinc chalcogenide are similar and relatively large, capable of simultaneously thermal-evaporating the solid-state substances. Specifically, a phase separation provides a compositional steepness at a hetero-interface between lead and zinc chalcogenide with a relatively large band-gap difference. To retain the most important characteristic of phase separation between lead and zinc chalcogenide, a technique of hot-wall deposition (HWD) should be employed due to a state near thermal equilibrium in a deposition atmosphere [10]. Based on these material designs, we proposed a composite thin film with PbSe nanocrystals embedded in a ZnSe matrix by one-step synthesis using HWD with multiple evaporation sources of PbSe and ZnSe [11]. Furthermore, this material design with these of HWD exhibits a unique characteristic of vapor-phase reaction. Evaporation sources of PbTe and ZnSe produce a nanocomposite containing ZnSe and nanocrystalline PbSe with slight inclusion of Te (PbSe:Te), transforming from PbTe (evaporation source) to PbSe:Te (film production) [12]. Different evaporation sources (PbSe or PbTe), therefore, provide similar nanocrystalline PbSe, but the XRD peaks of pure PbSe nanocrystals are weak even at a relatively high substrate temperature of 403 K [13], whereas nanoscale PbSe:Te crystallizes even at 274 K [12]. These results suggest that slight inclusion of Te in PbSe nanocrystal

✉ Seishi Abe  
abe@denjiken.ne.jp

<sup>1</sup> Research Institute for Electromagnetic Materials, 2-1-1 Yagiyama-minami, Sendai 982-0807, Japan

stabilizes the crystalline phase. Further investigation is needed whether pure PbTe nanocrystal actually stabilizes at a relatively low temperature. Moreover, a composite with PbSe nanocrystals embedded in ZnSe matrix exhibited n-type conductivity in our preliminary experiment, while compound semiconductor ZnTe tends to exhibit p-type conductivity [14]. Hence, composites with Pb and Zn chalcogenide system will possibly provide a p-n junction. Conductivity type should be investigated on ZnTe prepared by the HWD thus employed. Therefore, the present study employs a nanocomposite thin film with PbTe-ZnTe system. This system phase-separates at temperatures below 1160 K in bulk phase diagram [15]. Also, a nanocomposite thin film of PbTe nanocrystal embedded in a ZnTe matrix is capable of exhibiting quantum size effects because of the relatively large exciton Bohr radius of 46 nm in PbTe [16], and the relatively large band-gap difference between ZnTe (2.25 eV) [17] and PbTe (0.31 eV) [18] with type-I band offset [19]. Also, vapor pressure of PbTe [20] is similar to that of ZnTe [21]. Hence, simultaneous evaporation of solid-state sources (PbTe and ZnTe) is available for preparing a nanocomposite thin film with PbTe nanocrystals embedded in ZnTe matrix using HWD.

## Experimental

A nanocomposite thin film was prepared using HWD described elsewhere [11]. Here, PbTe and ZnTe were used as evaporation sources with 5N purity (Furuuchi Chemical, Tokyo, Japan). The two sources were located at different positions in a quartz liner to simultaneously thermal evaporate on a glass (Corning Eagle 2000, NY, USA) or Si substrate. The substrate temperature was changed by circulating water controlled at temperatures from 274 to 350 K. The temperatures were kept constant at 843 K for a source of ZnTe, and 683 K for the wall, which is located at another position without any source in the quartz liner. The temperature for a source of PbTe was varied from 713 to 778 K, to provide different PbTe concentrations. The film was structurally characterized using X-ray diffraction (XRD) with Cu K $\alpha$  radiation (Rigaku RAD-X, Tokyo, Japan). A symmetric  $2\theta$ - $\theta$  configuration was used. The composition of the film was analyzed using energy dispersive spectroscopy (EDS) (EDAX model, Phoenix, NJ, USA) operating at 10 kV with standard samples of PbTe to calibrate the analyzed results for Pb and Te, and with ZnSe for Zn. The Raman spectrum of the film was measured using a Raman spectrometer (JASCO NRS-5000, Tokyo, Japan) with a pumping semiconductor laser at 532 nm. The film was directly observed using transmission electron microscopy (TEM) operating at 300 kV (Hitachi

H-9000NAR, Tokyo, Japan). Ion milling was performed in the sample preparation. Current-voltage curve and photocurrent spectrum of the film were measured using photocurrent spectrometer (BUNKOUKEIKI, Tokyo, Japan).

## Results and discussion

Figure 1 depicts the XRD pattern of the thin films as a function of the concentration of Pb. In this case, the substrate temperature is kept constant at 350 K. Simultaneous evaporation enables multiple inclusions of elements (Pb, Zn, and Te), due to similar vapor pressures in PbTe [20] [ $\log(p/\text{atm}) = -11636T^{-1} + 7.946$ , where  $T$  is Kelvin temperature] and ZnTe [21] [ $\log(p/\text{atm}) = -10627T^{-1} + 6.771$ ]. The concentration of Pb can be controlled by the source temperature of PbTe. In the figure, a zinc-blende structure is first observed at 0.7 at.%Pb with dominantly [111] orientation despite the use of a glass substrate. A different phase with NaCl structure appears at 0.8 at.%Pb and any peak attributing to elements (Zn, Pb, and Te) cannot be seen in the pattern. Hence, the polycrystalline films form a phase mixture of zinc-blende structure and NaCl structure. The composition ratio in cation with Zn and Pb, and anion with Te tends to deviate Te-excess from stoichiometry in almost samples. In thermal evaporation of sources (PbTe and ZnTe), PbTe sublimates as a form of binary compound with species of 98 % in vapor phase [22] [ $\text{PbTe(s)} = \text{PbTe(g)}$ ], while ZnTe dissociates to each element [23] [ $\text{ZnTe(s)} = \text{Zn(g)} + 1/2\text{Te}_2\text{(g)}$ ]. Hence, a deviation from stoichiometry dominantly depends on the dissociated elements (Zn and Te). The Te-excess tendency suggests that the condensation coefficient of Te exceeds that of Zn.

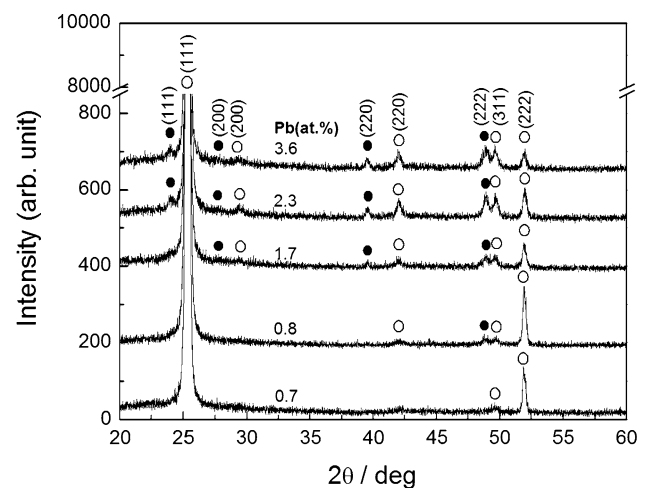
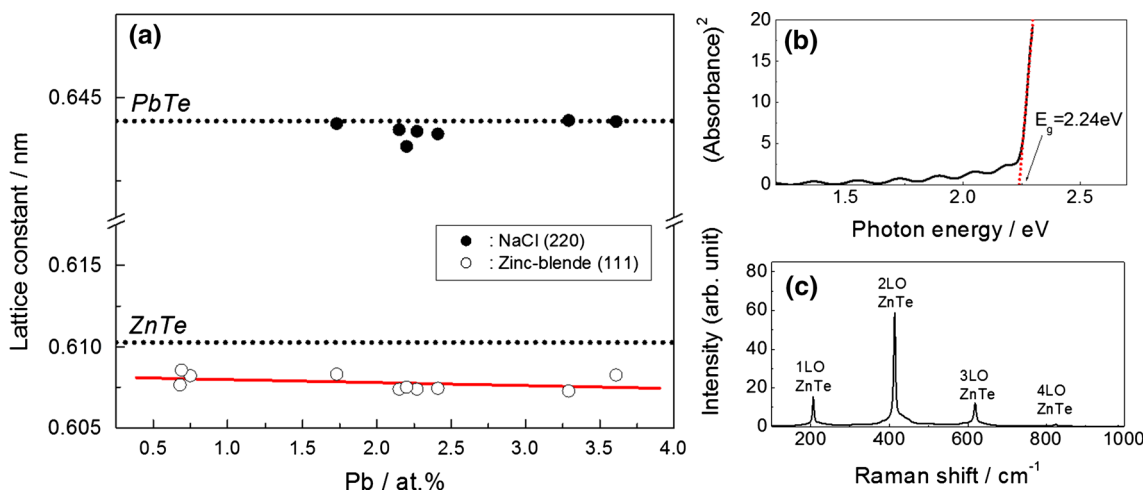


**Fig. 1** XRD pattern of thin films with respect to the source temperature of PbTe. *Black dots* indicate a phase with NaCl structure and *circles* indicate a phase with zinc-blende structure

Figure 2a depicts the lattice constant of the thin films as a function of the concentration of Pb. The lattice constant is estimated from the XRD peak at (111) Bragg reflection for zinc-blende structure and the peak at (220) for NaCl structure. The dotted lines indicate the lattice constants of standard ZnTe and PbTe. The lattice constant of the NaCl structure is almost the same to that of the standard PbTe regardless of the concentration of Pb. If a solid solution is formed in PbTe with element Zn, the lattice constant should decrease with increasing concentration of Pb, due to the difference in radii between Pb and Zn. Therefore, the phase with NaCl structure is reasonably assigned to PbTe. In the phase with zinc-blende structure, the lattice constant is slightly smaller than that of standard ZnTe and is almost unchanged regardless of the concentration of Pb. Figure 2b indicates the optical absorption spectrum of the thin film with 0.7 at.%Pb, 47.8 at.%Zn, and 51.5 at.%Te. The spectrum exhibits an optical absorption edge with an energy band gap of 2.24 eV, corresponding well to that of ZnTe (2.25 eV) [17]. Furthermore, Raman spectrum of the film (Fig. 2c) contains four peaks at  $206\text{ cm}^{-1}$  and its phonon replica is in good agreement with the Raman spectrum of ZnTe due to a longitudinal optical phonon mode (1LO) at  $206.5\text{ cm}^{-1}$  [24]. Hence, the phase with zinc-blende structure is reasonably assigned to ZnTe without alloying with Pb. Therefore, the thin films form a phase mixture of PbTe with NaCl structure and ZnTe with zinc-blende structure. The two compounds (PbTe and ZnTe) are therefore found to phase-separate even in the film production following the bulk phase diagram [15], during a simultaneous evaporation of solid-state sources (PbTe and ZnTe). This result also indicates that a deposition process using HWD provides a state with thermal equilibrium, since a preparation technique such as

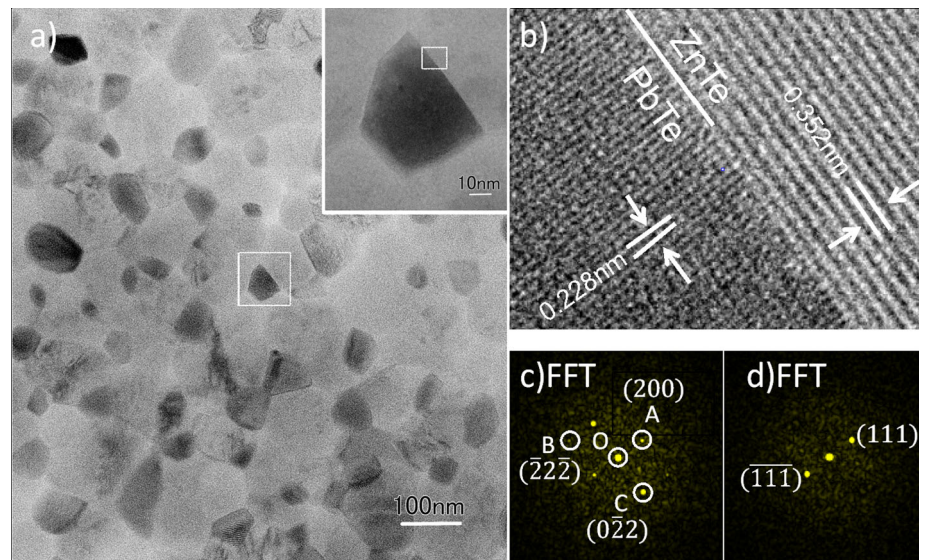
molecular beam epitaxy with thermally non-equilibrium provides a solid solution with a solubility range beyond that at thermal equilibrium [25].

Figure 3a presents a TEM plane view image of the thin film with 3.6 at.%Pb, 44.9 at.%Zn, and 51.5 at.%Te (i.e., about 7 at.%PbTe). The morphology is found to form a nanocomposite with slightly dark isolated nanoparticles dispersed in a bright matrix. The nanoparticles are well developed with sizes of 30–100 nm. In particular, it should be noted that faceted nanoparticles are frequently observed. The inset in Fig. 3a presents an enlarged image of typical faceted nanoparticle as denoted by the dotted line in Fig. 3a. A hetero-interface between the faceted nanocrystal and a crystalline matrix can be observed. The composite thin film forms polycrystalline structure (Fig. 1), but the geometric shape of the facet enables a fine observation of a lattice alignment at a nanoscale hetero-interface. Figure 3b represents high-resolution TEM image of the dotted square area in the inset in Fig. 3a. It is clearly found that the lattice fringes with plane widths of 0.228 nm at (0–22) in PbTe and 0.352 nm at (111) in ZnTe are perpendicularly aligned at the hetero-interface. The clear hetero-interface indicates that the two compounds phase-separate without forming an intermediate phase such as ternary solid solution  $\text{Zn}_{1-x}\text{Pb}_x\text{Te}$ . The strict change from PbTe to ZnTe at the hetero-interface (Fig. 3b) is expected to produce a steep energy potential barrier in PbTe nanocrystal for effectively confining an electron excited by absorbing light. Fast Fourier transform (FFT) analysis provides the details of the local alignment in the faceted nanoparticle. Figure 3c, d depicts the corresponding FFT diffraction pattern of the faceted nanocrystal and the matrix in Fig. 3b. The diffraction pattern can be indexed to cubic PbTe and ZnTe. In Fig. 3c, the diffractions with label-A, B, and C are assigned to



**Fig. 2** a Lattice constant of thin films as a function of the source temperature of PbTe. b Optical absorption spectrum and c Raman spectrum of a thin film with 0.7 at.%Pb

**Fig. 3** Direct observation of a thin film with 3.6 at.%Pb. **a** Plane view TEM image. *Inset* indicates an enlarged image of the *dotted* area. **b** High-resolution TEM image of the selected area denoted by *square* in the *inset* in **a**. **c** FFT diffraction pattern of the slightly dark nanocrystalline facet in **b**. **d** FFT diffraction pattern of the bright area in **b**



cubic PbTe with a plane width of 0.326 nm at (200), 0.185 nm at  $(-22-2)$ , and 0.228 nm at  $(0-22)$ . The angles A-O-B, A-O-C, and B-O-C are  $126^\circ$ ,  $89^\circ$ , and  $145^\circ$ , respectively. The lattice alignment of the nanocrystal corresponds to that of the standard data (JCPDS 38-1435), observing along the [011] direction. In Fig. 3d, the spots are assigned to the cubic ZnTe with a plane width of 0.352 nm at (111) and  $(-1-1-1)$ , corresponding well to the standard data in cubic ZnTe (JCPDS 15-0746). The results indicate that a growth direction of [111] in ZnTe aligns along that of [100] in PbTe. Furthermore, additional FFT-analysis (not shown here) also indicates [111] orientation in ZnTe matrix even at a different hetero-interface of [111] in the PbTe facet. Also, a pure ZnTe polycrystalline film exhibits a dominant growth orientation of [111] despite the use of a glass substrate in our preliminary experiment. Therefore, the ZnTe matrix at the hetero-interface (Fig. 3b) is reasonably considered to be an adhesive growth on the PbTe facet. It is considered as a kinetics of producing such alignment that a faceted PbTe nanocrystal is first developed on a film surface, and vaporized elements (Zn and Te) are subsequently deposited on the faceted PbTe [e.g., at (200)] for constructing a ZnTe compound (i.e., the facet just plays a role like a nanoscale substrate), since the solid-state sources dominantly evaporate as a form of binary compound in PbTe [22] and dissociate to each element in ZnTe [23]. The Te-excess tendency (Fig. 1) suggests that an element Te [i.e., (111)B] tends to first deposited on the PbTe facet prior to an element Zn [i.e., (111)A]. The faceted PbTe (inset in Fig. 3a) forms polyhedron shape. A nanocrystalline shape depends on a ratio of growth rate in [100] direction to that in [111] direction, forming cubic shape with a ratio of 0.58, and octahedron shape with a ratio of 1.73 [26]. The size of

{200} facet in the inset in Fig. 3a exceeds that of  $\{-22-2\}$  facet. This result suggests that the ratio of growth rate in the faceted PbTe nanocrystal is less than 1 during the simultaneous evaporation with PbTe and ZnTe. A ratio of growth rate in ZnTe to that in PbTe will also affect the shape of faceted PbTe nanocrystal, while the present study employs relatively low inclusion (i.e., low growth rate) of PbTe (Fig. 1). It is, therefore, found that one-step synthesis provides a nanocomposite thin film with faceted PbTe nanocrystals embedded in ZnTe matrix, with clear phase separation at hetero-interface.

In our previous study, a composite with PbSe nanocrystals embedded in ZnSe matrix exhibited n-type conductivity, whereas a compound semiconductor ZnTe tends to exhibit p-type conductivity [24]. Hence, composites with Pb and Zn chalcogenide system will possibly provide a p-n junction. Conductivity type is next investigated on ZnTe employed as the matrix in the nanocomposite thin film. Figure 4a depicts current-voltage curves of ZnTe thin films prepared on Si substrate with n-type and p-type conductivity using HWD with an evaporation source of ZnTe without PbTe. ITO electrode with 20 nm-thick is deposited on the ZnTe thin films and In-electrode is contacted to Si substrate as indicated in the inset. The ZnTe thin film on p-type Si exhibits rectifying behavior in the dark and photovoltaic characteristic with an open circuit voltage of 0.12 V under irradiation of solar simulator (AM1.5), whereas the ZnTe thin film on n-type Si provides a weak behavior in the dark. This result suggests that the ZnTe thin film has n-type conductivity. Hence, p-type Si is employed as a substrate for preparing the nanocomposite thin films to investigate photocurrent spectrum. Figure 4b depicts typical normalized photocurrent spectra of the nanocomposite thin films prepared at a substrate

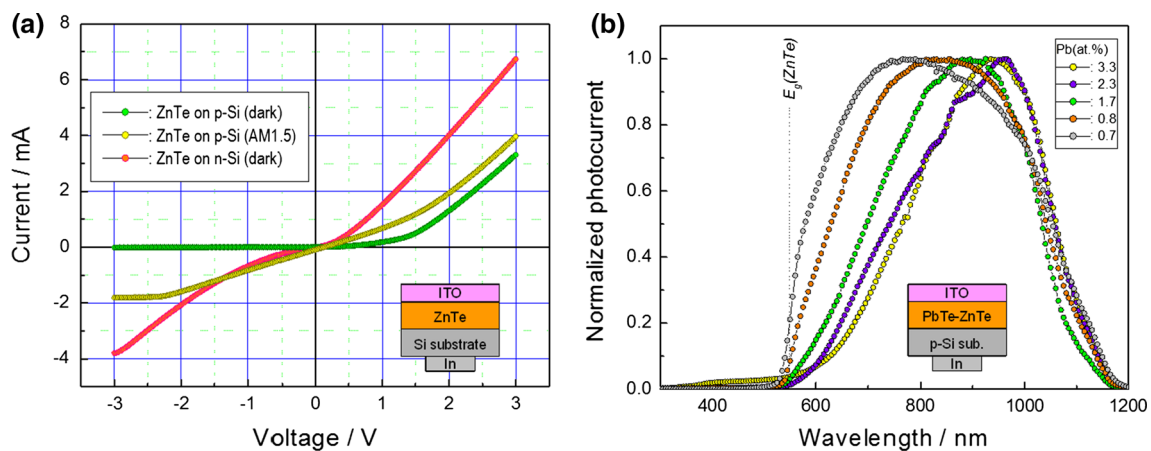


**Fig. 4** **a** Current–voltage curve of ZnTe thin films and **b** normalized photocurrent spectrum of nanocomposite thin films

temperature of 350 K. The broad spectra can be observed in the wavelength range. The photocurrent generates at wavelengths exceeding 549 nm as indicated by dotted line (energy band gap of ZnTe) and wavelengths below 1200 nm that is considerably apart from the energy band gap of PbTe (4000 nm). The PbTe nanocrystals exhibit no obvious quantum size effects due to their relatively large size (Fig. 3). Hence, the photocurrent reasonably depends on Si substrate. The normalized photocurrent decreases in visible wavelength range with increasing Pb concentration. This result indicates that an increase of PbTe nanocrystals with relatively large size in the nanocomposite reduces a photoresponse in visible range. Doping impurity will be needed to prepare p-type ZnTe.

Next, temperature dependence of substrate is investigated to clarify temperature stability of PbTe nanocrystals embedded in ZnTe matrix. Figure 5a depicts the XRD pattern of nanocomposite thin films with respect to substrate temperature. In this case, Pb concentration is kept constant at  $5.3 \pm 0.5$  at.% (except the sample at 274 K with 1.4 at.%Pb), since mean grain size of PbTe minimizes at 5.3 at.%Pb with respect to Pb concentration in the range from 1.7 to 6.1 at.% in our preliminary experiment. Hence, most of the nanocomposite thin films are expected to contain about 10 at.%PbTe. The dotted line indicates the peak position of standard PbTe and ZnTe. The diffraction peaks in PbTe with NaCl structure and ZnTe with zincblende structure are clearly observed at 274 K. Hence, the composite film with PbTe nanocrystals embedded in ZnTe matrix is crystallized even at a relatively low temperature of 274 K. In our previous study, the XRD peak of PbSe in the PbSe–ZnSe composite thin films is weak even at the relatively high temperature of 403 K [13]. Furthermore, nanoscale PbTeSe ternary solid solution crystallizes at a substrate temperature of 274 K in a composite film with ZnSe matrix [12]. The present result (Fig. 5a) strongly suggests that an inclusion of Te in PbSe stabilizes a

nanocrystalline state embedded in ZnSe matrix at relatively low temperature. The mean grain size of PbTe is depicted in Fig. 5b. The mean grain size is estimated from the full width at half maximum of the diffraction peak, according to Scherrer's formula [27]. The size varies from 22 to 13 nm with respect to the substrate temperature, but there is no obvious tendency. It is, therefore, found in the PbTe–ZnTe nanocomposite thin films that both the compounds crystallize even at a substrate temperature of room temperature without any post-annealing.

One-step synthesis provides a nanocomposite thin film with faceted PbTe nanocrystals embedded in ZnTe matrix during simultaneous evaporation of solid sources (PbTe and ZnTe) with similar vapor pressures. The composite has a strict hetero-interface between PbTe and ZnTe, without forming a ternary solid solution such as  $\text{Zn}_{1-x}\text{Pb}_x\text{Te}$ . Hence, PbTe nanocrystal is expected to form a steep energy potential barrier with type-I band offset [19]. According to Brus model [28], the ground state transition of electron–hole pairs in PbTe nanocrystal is calculated to be 0.38 eV with a mean grain size of 13 nm at 290 K, which is the smallest size thus obtained in the present study. The estimated band gap is close to that of bulk PbTe (0.31 eV). The nanocomposite thin film actually exhibits broad optical absorption toward infrared range. This broad absorption suggests that quantum size effects are weak in the PbTe nanocrystals. Further decrease in grain size of PbTe nanocrystals is therefore needed to enhance quantum size effects.

## Conclusion

We investigated one-step synthesis of a nanocomposite thin film with faceted PbTe nanocrystals embedded in ZnTe matrix using HWD with solid-state sources (PbTe and ZnTe). Similar vapor pressures in the two compounds

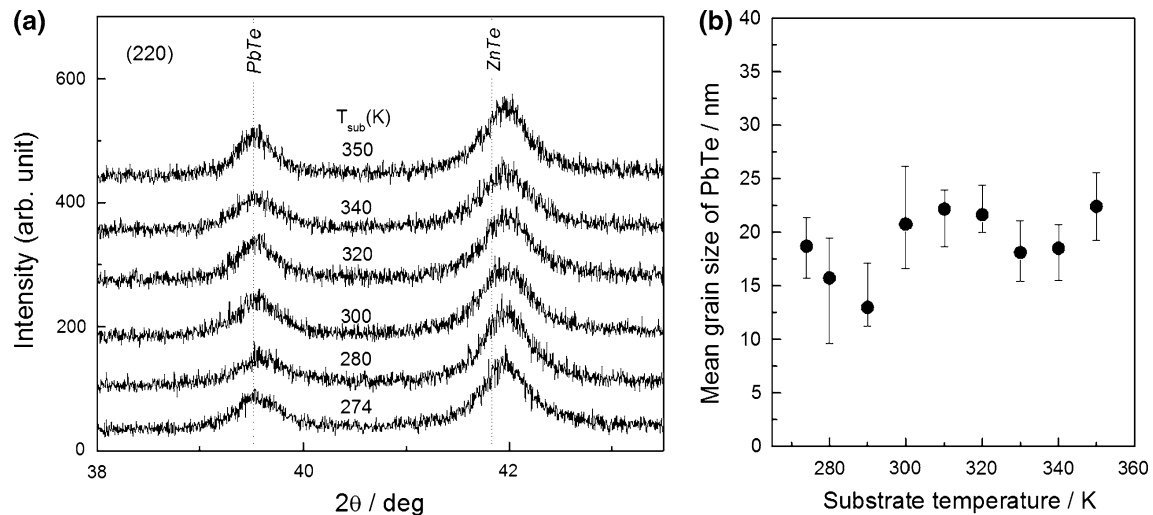


**Fig. 5** XRD pattern of nanocomposite thin films with respect to substrate temperature. **a**  $2\theta$  range from  $38^\circ$  to  $43.5^\circ$ . The dotted lines indicate the peak positions of standard PbTe and ZnTe. **b** Mean grain

size of PbTe estimated from the diffraction peak of PbTe (**a**) as a function of the substrate temperature

enable simultaneous evaporation in addition to a compositional control of PbTe. The compounds phase-separate at the hetero-interface without forming an intermediate phase such as ternary solid solution  $\text{Zn}_{1-x}\text{Pb}_x\text{Te}$ . Also, a faceted PbTe nanocrystal forms polyhedron shape in ZnTe matrix. The ZnTe tends to grow [111] direction at the hetero-interface. The nanocomposite crystallizes even at 274 K (i.e., enabling a preparation at room temperature without post-annealing), exhibiting temperature stability at relatively low substrate temperature. Current–voltage curve suggests that the ZnTe thin film prepared by the HWD apparatus exhibits n-type conductivity. Doping impurity will be needed for preparing p–n junction using lead and zinc chalcogenide system.

**Acknowledgments** The present work was supported by a Grant-in-Aid for Scientific Research from the Japan Society for the Promotion of Science (No. 24360295). The author gratefully acknowledges the valuable comments of Grand-Fellow T. Masumoto [Research Institute for Electromagnetic Materials (DENJIKEN), Sendai, Japan]. The author is also grateful to Mr. N. Hoshi (DENJIKEN) and Ms. S. Sato (DENJIKEN) for assisting in the experiments.

**Open Access** This article is distributed under the terms of the Creative Commons Attribution 4.0 International License (<http://creativecommons.org/licenses/by/4.0/>), which permits unrestricted use, distribution, and reproduction in any medium, provided you give appropriate credit to the original author(s) and the source, provide a link to the Creative Commons license, and indicate if changes were made.

## References

- Nozik, A.J.: Quantum dot solar cells. *Phys E* **14**, 115–120 (2002)
- Liu, D., Kamat, P.V.: Photoelectrochemical behavior of thin CdSe and coupled  $\text{TiO}_2/\text{CdSe}$  semi-conductor films. *J Phys Chem* **97**, 10769–10773 (1993)
- Weller, H.: Quantum sized semiconductor particles in solution in modified layers. *Ber Bunsenges Phys Chem* **95**, 1361–1365 (1991)
- Zhu, G., Su, F., Lv, T., Pan, L., Sun, Z.: Au nanoparticles as interfacial layer for CdS quantum dot-sensitized solar cells. *Nanoscale Res Lett* **5**, 1749–1754 (2010)
- Hoyer, P., Könenkamp, R.: Photoconduction in porous  $\text{TiO}_2$  sensitized by PbS quantum dots. *Appl Phys Lett* **66**, 349–351 (1995)
- Chatterjee, S., Goyal, A., Shah, I.: Inorganic nanocomposites for next generation photovoltaics. *Mater Lett* **60**, 3541–3543 (2006)
- Yang, W., Wan, F., Chen, S., Jiang, C.: Hydrothermal growth and application of ZnO nanowire films with ZnO and  $\text{TiO}_2$  buffer layers in dye-sensitized solar cells. *Nanoscale Res Lett* **4**, 1486–1492 (2009)
- Abe, S., Ohnuma, M., Ping, D.H., Ohnuma, S.: Anatase-dominant matrix in  $\text{Ge}/\text{TiO}_2$  thin films prepared by RF sputtering method. *Appl Phys Exp* **1**, 095001 (2008)
- Abe, S.: InSb-added  $\text{TiO}_2$  nanocomposite films by RF sputtering. *Nanoscale Res Lett* **8**, 269 (2013)
- Lopez-Otero, A.: Hot wall epitaxy. *Thin Solid Films* **49**, 3–57 (1978)
- Abe, S.: One-step synthesis of PbSe–ZnSe composite thin film. *Nanoscale Res Lett* **6**, 324 (2011)
- Abe, S.: One-step synthesis of composite thin film with ZnSe and PbTeSe ternary solid solution. *Mater Renew Sustain Energy* **4**, 18 (2015)
- Oba, Y., Abe, S., Ohnuma, M., Sato, N., Sugiyama, M.: Temperature dependence of nanostructure in PbSe–ZnSe composite thin film. *J Phys D Appl Phys* **47**, 435102 (2014)
- Title, R.S., Mandel, G., Morehead, F.F.: Self-compensation-limited conductivity in binary semiconductors. *Phys Rev* **136**, A300 (1964)
- Grytsiv, V.I., Tomashik, V.N., Olejnik, G.C., Tomashik, Z.F.: Investigation of the ZnTe–PbTe system [in Russian]. *Izv AN SSSR Neorg Mater* **16**, 543–544 (1980)
- Wise, F.W.: Lead salts quantum dots the limit of strong confinement. *Acc Chem Res* **33**, 773–780 (2000)

17. Nahory, R.E., Fan, H.Y.: Optical properties of zinc telluride. *Phys Rev* **825**, 156 (1967)
18. Zemel, J.N., Jensen, J.D., Schoolar, R.B.: Electrical and optical properties of epitaxial films of PbS, PbSe, PbTe, and SnTe. *Phys Rev* **140**, A330–A342 (1965)
19. Rawat, P.R., Paul, B., Banerji, P.: Exploration of Zn resonance- and thermoelectric properties in I-doped PbTe with ZnTe nanostructures. *ACS Appl Mater Interfaces* **6**, 3995–4004 (2014)
20. Pashinkin, A.S., Novoselova, A.V.: Opredelenie davleniya nasyshchennogo para tverdogo telluridasvintsa [in Russian]. *Zhur Neorg Khim* **4**, 2657–2660 (1959)
21. Korneeva, I., Belyaev, A.V., Novoselova, A.V.: Determing saturated vapor pressure of solid zinc and cadmium tellurides [in Russian]. *Zhur Neorg Khim* **1**, 5–12 (1960)
22. Brebrick, R.F., Straus, A.J.: Partial pressures in equilibrium with group IV tellurides. I. Optical absorption method and results for PbTe. *J Chem Phys* **40**, 3230–3241 (1964)
23. Goldfinger, P., Jeunehomme, N.: Mass spectrometric and Knudsen-cell vaporization studies of group 2B-6B compounds. *Trans Faraday Soc* **59**, 2851–2867 (1963)
24. Liu, N.Z., Li, G.H., Zhu, Z.M., Han, H.X., Wang, Z.P., Ge, W.K., Sou, I.K.: Raman scattering and photoluminescence of  $ZnS_xTe_{1-x}$  mixed crystals. *J Phys Condens Matter* **10**, 4119–4129 (1998)
25. Koguchi, N., Kiyosawa, T., Takahashi, S.: Double hetero structure of  $Pb_{1-x}Cd_xS_{1-y}Se_y$  lasers grown by molecular beam epitaxy. *J Cryst Growth* **81**, 400–404 (1987)
26. Wang, Z.L.: Transmission electron microscopy of shape-controlled nanocrystals and their assemblies. *J Phys Chem* **104**, 1153–1175 (2000)
27. Guinier, A.: X-ray diffraction in crystals, imperfect crystals, and amorphous bodies. Dover Publications, Mineola (1994)
28. Brus, L.E.: A simple model for the ionization potential, electron affinity, and aqueous redox potentials of small semiconductor crystallites. *J Chem Phys* **79**, 5566–5571 (1983)